

Experimental investigations of the effect of thickness on fracture toughness of metallic foils

Yi-Lan Kang^{a,*}, Zhi-Feng Zhang^a, Huai-Wen Wang^a, Qing-Hua Qin^b

^a School of Mechanical Engineering, Tianjin University, Tianjin 300072, PR China

^b Department of Engineering, Australian National University, Canberra, ACT 0200, Australia

Received 2 August 2004; received in revised form 15 November 2004; accepted 17 November 2004

Abstract

The effect of thickness on the fracture toughness J_C of metallic foil was investigated experimentally. Double-edge cracked specimens, made of copper foils with thicknesses t ranging from 0.02 to 1 mm, were loaded in tension till fracture. The digital speckle correlation method (DSCM) was used to evaluate the strain fields around the crack tip, allowing determination of the J integral. The fracture toughness defined as the value of the J integral at cracking initiation was shown to first increase with increasing thickness, then to reach a maximum for a thickness of about 0.3 mm and finally to decrease at larger thicknesses. Optical and scanning electron microscopy (SEM) results showed that this significant effect of thickness is essentially attributable to the change in the work required per unit area during crack tip necking and in the work required per unit area during material separation.

© 2004 Elsevier B.V. All rights reserved.

Keywords: Fracture toughness; Thickness effect; Metallic foil; Digital speckle correlation method

1. Introduction

With the rapid development of modern technology, foil materials have found applications in the areas of materials and electrical industries such as microelectro-mechanical systems (MEMS) and integrated circuits. The mechanical behavior of such materials may be different from that of bulk materials due to size effects. Therefore, models and conclusions appropriate for bulk materials may not be applicable when analyzing foil materials. Certain essential problems and phenomena occurring during the fracture process of foils must be explored by experiments and numerical simulation methods in order to provide a better understanding of fracture mechanisms, especially their difference from bulk materials. For example, the effect of the thickness of the foils on the fracture behavior remains an open issue.

During last two decades, several investigations of the mechanical properties of foils have been carried out both ex-

perimentally and theoretically. For example, Sutton et al. [1] measured the near tip surface deformation fields, evaluated the J integral, and investigated the three-dimensional effects near the crack tip in thin sheet using computer vision. Judelewicz et al. [2] and Arzt [3] demonstrated that size effect on the material properties of foil materials was attributed to dimensional and microstructural constraints. Fan [4] made an assessment of the grain size dependence of ductile fracture toughness using available experimental data from various metals and alloys and proposed a semi-empirical equation. Also, the grain size dependence of ductile fracture toughness was discussed in terms of the influence of yield strength and strain to fracture, as well as of the effect of deformation homogeneity across the grain. Further research regarding size effect on fatigue behavior of thin films has shown that the mechanical behavior was closely related to the thickness and grain size of the films [5–9]. Klein et al. [10] studied the stress–strain behavior of thin metallic foils of Cu and Al with varying thickness ranging between 10 and up to 250 μm and the fatigue crack propagation properties of the above mentioned Cu foils as function of thickness. Results of the fracture topography

* Corresponding author. Tel.: +86 22 87894001; fax: +86 22 87894001.
E-mail address: ylkang@public.tpt.tj.cn (Y.-L. Kang).

showed that the size effect resulting in an influence mainly on the fracture strain might be explained on the basis of texture differences, the number of activated gliding systems as a dependence on the ratio of grain size to foil thickness. Choi and Suresh [11] analyzed size effect on the mechanical properties of thin polycrystalline metal films, and developed a model that correctly predicts the observed influence of film thickness and grain size on stress evolution during thermal excursions. Pardoen et al. [12,13] investigated size effect on the fracture toughness of aluminum thin plates of 1–6 mm thickness from tensile testing of double-edge notched tension (DENT) specimens. Their research showed that thickness indeed influences fracture toughness, and the critical J integral and critical crack tip opening displacement (CTOD) constitute equivalent measures of fracture toughness at small thickness. More recently, relations between fracture toughness and microstructural details have been calculated for ductile materials based on a dilatational plasticity constitutive model which generalizes the Gurson model to account for both void growth and coalescence with explicit dependence on void shape and distribution effects [14]. Kang and co-workers [19,20] measured and calculated the fracture toughness of copper foil along several contours by an improved digital speckle correlation method (DSCM). Yang [21] derived an analytical solution of the load–displacement relationship for the indentation problem of an elastic layer by a rigid flat-ended cylindrical indenter. In addition, the effect of adhesion between the elastic layer and the indenter was addressed and an analytical solution of the pull-off force was obtained. Results showed that the pull-off force is a function of the layer thickness and Poisson's ratio. It increases with Poisson's ratio and the ratio of the contact radius to the layer thickness. Kotousov and Tan [22] presented analytical results on the out-of-plane displacement of the lateral surface of a plate in the vicinity of a through-the-thickness crack at different ratios of the crack length to the plate thickness.

From the above review, we note that most of the existing work has focused on mechanical size effects in thin films whose thickness was usually greater than 1 mm or less than 1 mm but supported by a substrate. Nowadays, many modern electronic devices or packages involve very thin “free-standing” films (usually much thinner than 1 mm) for which the mechanical and fracture behaviors are critical in analyzing the performance of whole structure. However, there is a lack of knowledge on the complex size effect in such foils that is required for optimal design and manufacture. The present work aims at addressing this problem. The DSCM as previously established [15–20] is used to obtain the displacement and strain fields near the crack tip region, allowing determination of the fracture toughness, characterized by J_C and defined as the value of the J integral at cracking initiation, of specimens with thicknesses ranging from 20 μm to 1 mm. Then macroscopic and microscopic examinations by optical and scanning electron microscopy (SEM) are used to explore the fracture profile as well as the specimen surface of the copper foils. The influence of thickness effect and microstruc-

ture on the fracture toughness of the foil is discussed in detail.

2. Experimental procedure

2.1. Material properties

The specimens employed in this study were made of T2 copper foil with thicknesses ranging from 20 μm to 1 mm. All specimens were produced by the same processing technology, and thus had the same chemical composition and content. The Young's modulus E and Poisson's ratio μ of the material were about 108.5 GPa and 0.334, respectively. A Ramberg–Osgood relation was used to fit the uniaxial stress–strain data, which were measured by the CSS-44100 experimental machine. The functional form is written as

$$\frac{\varepsilon}{\varepsilon_0} = \frac{\sigma}{\sigma_0} + \alpha \left(\frac{\sigma}{\sigma_0} \right)^n \quad (1)$$

where α is the strain-hardening exponent, n the strain-hardening exponent, σ_0 and ε_0 are the flow stress and strain, respectively. By the least square method, we obtain $\alpha = 0.0288$ and $n = 15.47$. Good agreement was found between the fitted curves of the Ramberg–Osgood equation and the original uniaxial stress–strain curves [20].

2.2. Fracture tests

In the fracture experiments, the thin foils with different thicknesses were processed in the same way and all are with double-edge cracks. The dimensions are shown in Fig. 1. The crack on each specimen was made as follows: a line-incisor with a radius of 0.1 mm was used to make an initiatory crack and then a sharp razor was used to make the crack tip. The radius of the razor was approximately 25 μm . The validity of this pre-cracking method has been justified by Pardoen et al. [12]. The specimens were classified into H-specimens and V-specimens, according to the relationship between the

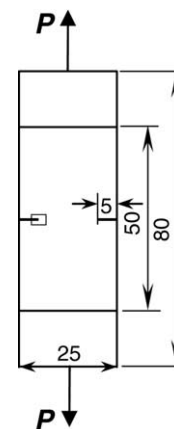


Fig. 1. Dimensions of the specimen and location of cracks.

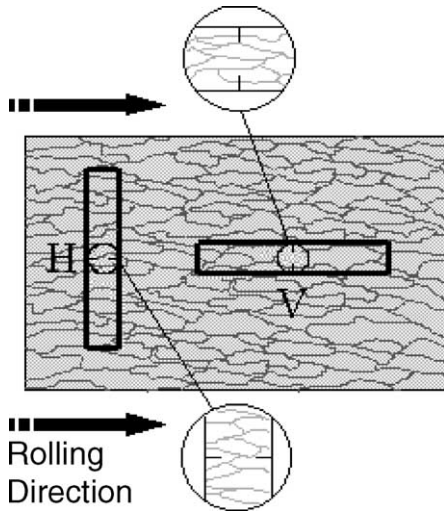


Fig. 2. Scheme showing the orientation of the specimen with respect to rolling direction and grain flow.

rolling direction and the crack path (see Fig. 2). H-specimens were those with a crack path parallel to the rolling direction; V-specimens were those with a crack path perpendicular to the rolling direction.

The DSCM (also known as digital image correlation method) was used in this work for measuring the fracture toughness J_C of the specimens. The process in DSCM includes recording, digitizing and processing two speckle patterns (or images) of an object in two different deformation states to yield in-plane displacement components and in-plane displacement gradients. The two speckle images of the surface of the object are usually captured before and after loading. The speckle images in the two states are known as reference and deformed speckle patterns, respectively. A small speckle area in the undeformed speckle pattern is taken as a reference subset and the speckle area corresponding to the reference subset in the deformed speckle pattern is defined as the target subset. In this case, it is essential to identify the corresponding relation between the two subsets. Differences between the two subsets include translation and distortion information about the object. The deformation measurement is performed at two different deformation stages and comparison is made for subsets between the two digital patterns. Finally, the J integral can be calculated based on the strain field in the region around the crack tip, using

$$J = \frac{1}{2} \int_{\Gamma} \left[\frac{E}{1-\mu^2} \left(\frac{\partial u}{\partial x} + \mu \frac{\partial v}{\partial y} \right) \frac{\partial u}{\partial x} + \frac{E}{1-\mu^2} \left(\frac{\partial v}{\partial y} + \mu \frac{\partial u}{\partial x} \right) \frac{\partial v}{\partial y} + G \left(\frac{\partial u}{\partial y} + \frac{\partial v}{\partial x} \right)^2 \right] dy - \int_{\Gamma} \left[\frac{E}{1-\mu^2} \left(\frac{\partial u}{\partial x} + \mu \frac{\partial v}{\partial y} \right) \frac{\partial u}{\partial x} + G \left(\frac{\partial u}{\partial y} + \frac{\partial v}{\partial x} \right) \frac{\partial v}{\partial x} \right] dy + \int_{\Gamma} \left[\frac{E}{1-\mu^2} \left(\frac{\partial v}{\partial y} + \mu \frac{\partial u}{\partial x} \right) \frac{\partial v}{\partial x} + G \left(\frac{\partial u}{\partial y} + \frac{\partial v}{\partial x} \right) \frac{\partial u}{\partial x} \right] dx \quad (2)$$

where Γ is an anticlockwise curve that surrounds the crack-tip, u and v are the components of the displacement vector in the x - and y -direction, respectively. In our calculation, the integral path forms a symmetrical rectangle as shown in Fig. 3.

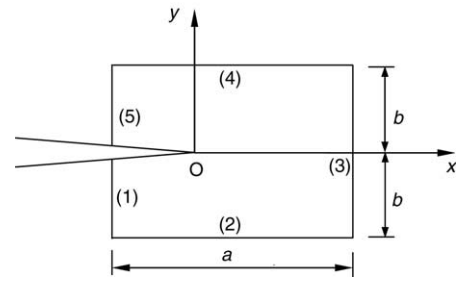


Fig. 3. Rectangular symmetrical integral path.

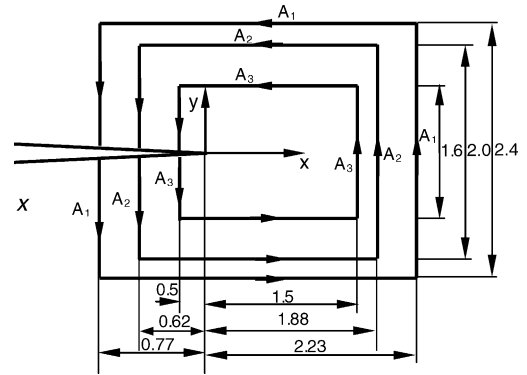


Fig. 4. Dimensions of rectangular integral contours.

Thus, the J integral can also be written in the form

$$J = J_{(1)} + J_{(2)} + J_{(3)} + J_{(4)} + J_{(5)} \quad (3)$$

where $J_{(i)}$ stands for the value of J along the path i (see Fig. 3). Detailed derivation of J integral is provided in Appendix A of this paper for the reader's convenience. In this work, multiple rectangular contours with varying dimensions were used to calculate the J integral. Results indicated that J integral is stable when the contours are not too close to the crack tip. As illustrated in Fig. 4, the contours we had taken are: (1) $a=3$, $b=1.2$; (2) $a=2.5$, $b=1$ and (3) $a=2$, $b=0.8$. It is found that results of (1) and (2) were in agreement with each other. And the result corresponding to (3) was a little bit deviated from the previous two cases.

For accurately determining the value of J_C , i.e., J integral when the crack tip initiated, a double charge coupled device (CCD) system equipped with zooms (Fig. 5) was designed to accurately determine the value of J_C . One CCD

system was used to observe the crack tip in real time and another to serially capture the digital speckle pattern. The pattern captured just before crack tip initiation was taken as

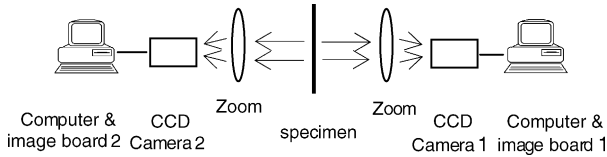


Fig. 5. CCD system.

the deformed image. The experimental method of J_C evaluation is schematically summarized in Fig. 6. It is well known that one important requirement of any fracture toughness test is the ability to detect the initiation of fracture. Several methods have been described in the literature. Here we refer to the method given by EI-Soudani [23], namely thumbnails technique, because the precision of this technique is high enough for our experimental purpose and can be used in the experimental research step by step. Moreover, it has been used by many other researchers.

In order to apply the load, a load frame was used. Each end of the specimen was first mounted into clamp, and then one of the clamps was fixed at the bottom of the frame while the other was attached to a screw and displaced. In this work, the screw was located approximately three specimen widths away from the crack and crossed the symmetric axis of the specimen. Therefore, the loading is approximated as a remote, uniform, uniaxial tensile stress. In order to measure the force applied by the displacement, the displaced clamp was attached to a load cell. However, it should be noted that the J integral is directly calculated from the strain fields around the crack tip evaluated by DSCM, without using the loading values. The loads applied to all the specimens with different thickness were recorded when the crack tip initiated for reference (not given in the paper).

2.3. Metallographic examinations

The experiment in this work also includes metallographic examinations of the specimen surface and fracture profile

by optical microscopy and SEM. In particular, the surface and fracture profile of the specimens, including the amount of roll marks, the degree of crack-tip necking and the macro-appearance, were observed by optical microscopy before and after deformation. The microstructural features of the fracture profile were examined by SEM (Philips, XL30 ESEM). These tests were performed at room temperature.

3. Experimental results

3.1. Toughness/thickness curve

Based on DSCM experimental results, the fracture toughness J_C of the specimens is presented in Fig. 7 as a function of specimen thickness, showing that J_C strongly depends on thickness. In a so-called stage I (see Fig. 7), J_C is shown to increase with an increase in thickness, then to reach a maximum at the thickness $t \approx 0.3$ mm. Conversely, J_C decreases as the thickness increases within the so-called stage II and the decreasing rate becomes slowdown along with an increase in thickness (see Fig. 7). It is also evident that the J_C values

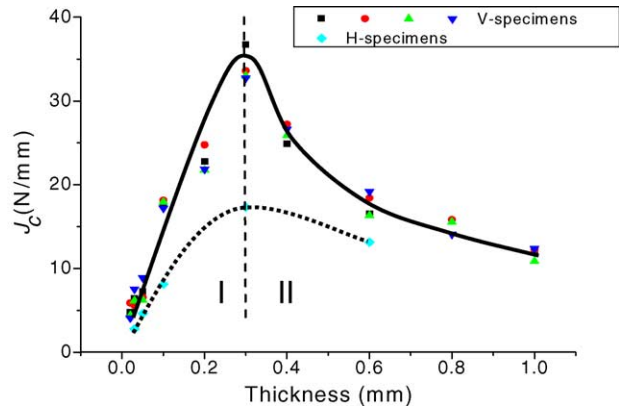


Fig. 7. Relation between J_C and thickness.

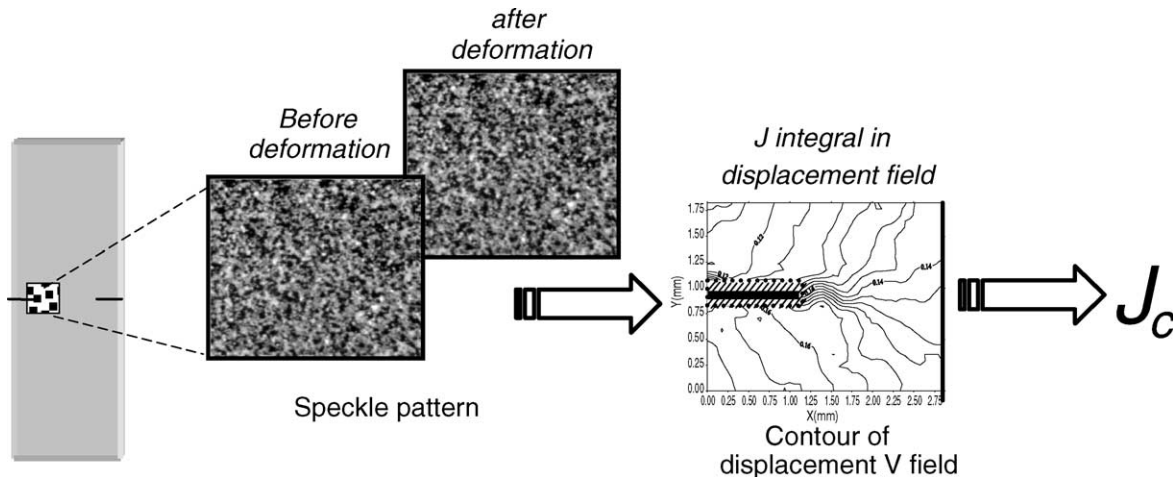


Fig. 6. Schematic illustration of J_C evaluation processing.

of the V-specimens are always greater than those of the H-specimens at any given thickness. Moreover, it should be noted that Fig. 7 is similar to the plots presented in many textbooks such as that of Kanninen and Popelar [24].

3.2. Results of metallographic examinations

The specimen surface and fracture profile were firstly examined by optical microscopy. Results show that the degree of necking at the crack tip increases with increasing thickness in stage I, while decreases with increasing thickness in stage II. Besides, the surface showed evidence of roll marks along the rolling direction, and the grains are also elongated along the rolling direction (Fig. 2).

In addition, the fracture surface was inspected by SEM in order to characterize the micro-mechanisms of the fracture and the micro-fracture appearance in front of the crack tip. Results of the micro-fractographs (see Figs. 8–10) show that important differences exist between deformation behavior of thin and thick foils. Detail descriptions are as follows.

Fig. 8(a–d) presents the SEM micro-fractographs in stage I. It can be seen that specimens with the smallest thickness (Fig. 8(a)) show that brittleness occurs with shear mode fracture feature. The specimen with a thickness of 0.1 mm shows shear mode as well as dimple–ductile fracture features, with shallow dimples elongated in the direction pointing to the surface (Fig. 8(b)). Specimens with thickness ranging from 0.2 to 0.3 mm show ductile fracture features with slip bands and lenticular dimples (Fig. 8(c and d)). Additionally, in the case of ductile fracture (Fig. 8(c and d)), as the thickness in-

creases, the amount of slip bands, tear ridges and the size of the dimples all increase, and the dimples become deeper. This indicates that the fracture mechanism changes from a mixed brittle/shear-mode fracture to a mixed shear-mode/ductile fracture, and then to a mixed ductile fracture with slip bands, tear ridges and lenticular dimples.

Fig. 9(a–d) demonstrates the SEM micro-fractographs in stage II. They illustrate that the fracture mechanism changes from mixed ductile fracture with slip bands, tear ridges and lenticular dimples (Fig. 9(a and b)) to mixed ductile fracture with tear ridges and well-developed equiaxed dimples only (Fig. 9(c and d)). Moreover, the fractographs show that the dimple diameter and depth become respectively larger and deeper as the thickness increases. However, the amount of slip bands and tear ridges decreases with an increase in thickness.

4. Discussion

4.1. Macroscopic and microscopic fracture features

It is considered that the changes in the crack-tip necking degree, the dimple diameter and depth, the amount of slip bands and tear ridges, and the fracture mechanism are mainly due to the influence of a reduction in micro-defects (i.e. roll marks on the surface and defects caused by rolling), an increase in the plastic deformability of the material itself and an increase in stress triaxiality.

In stage I, the major affecting factors are the influence of a reduction in micro-defects and an increase in the plastic

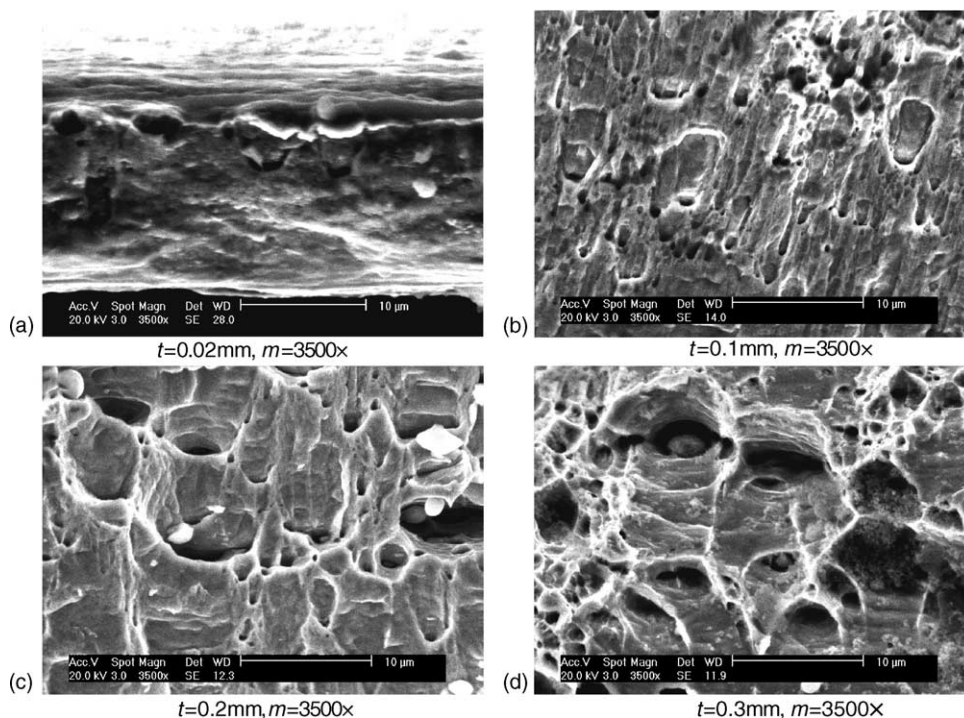


Fig. 8. SEM micro-fractographs at stage I; t and m denote thickness and magnification, respectively.

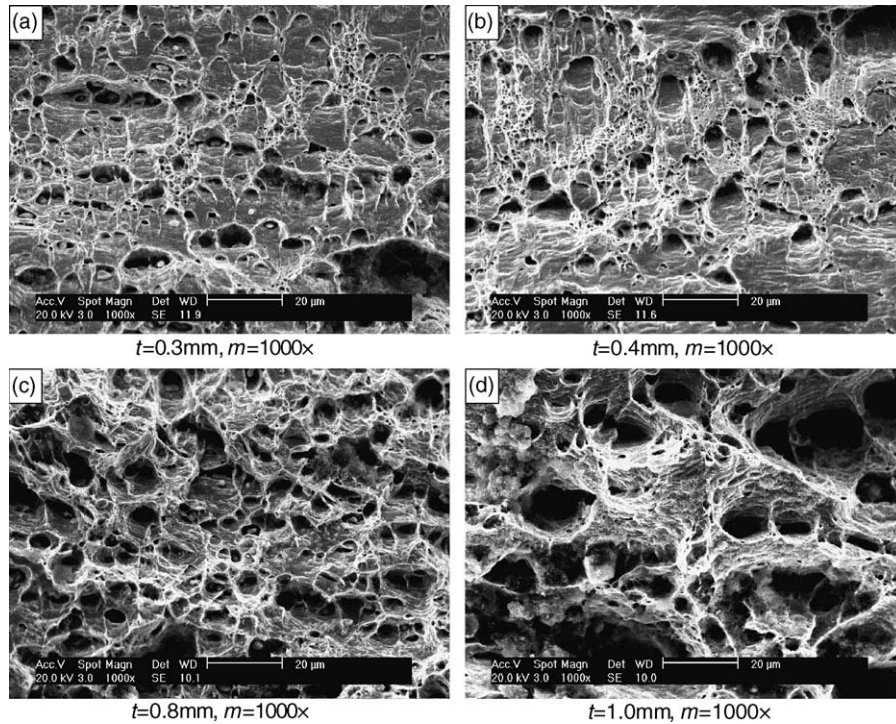


Fig. 9. SEM micro-fractographs at stage II; t and m denote thickness and magnification, respectively.

deformability of the material itself, for the influence of the stress triaxiality associating with the plane stress tension situation is assumed to be negligible when thickness is very small. The thinnest specimen shows brittleness occurring with a shear mode fracture pattern with no necking degree, probably because the micro-defects affect greatly the fracture behavior of the thin film at the lowest thickness. It is also possible that fracture is easier caused by micro-defects than slip, which caused the fracture before the slip had completed. Then as

the thickness increases, the influence of the micro-defects reduces but the deformability of the specimen increases. This results in an increase of the crack-tip necking degree and a change in the fracture mode, from a more brittle mechanism to a more ductile mechanism involving void growth.

In stage II, the influence of the micro-defect might be negligible for the thickness is large enough, and thus the dominant factors should be stress triaxiality and plastic deformability of the material itself. With increasing thickness, stress triaxiality will tend to increase at the crack tip, to accelerate the void growth rate with respect to the plane strain tension situation, to increase the deformation resistance and thus lead to a decrease in the fracture strain, crack-tip necking degree and the amount of slip bands when crack extension begins. The increase of the dimple diameter and depth can be attributed to the increase in the plastic deformability of the material and the fact that void growth is favored by higher stress triaxiality, and hence may lead to a decrease in the amount of tear ridges and a change in the fracture mechanism from mixed ductile fracture with slip bands, tear ridges and lenticular dimples (Fig. 9(a and b)) to mixed ductile fracture with tear ridges and well-developed equiaxed dimples only (Fig. 9(c and d)).

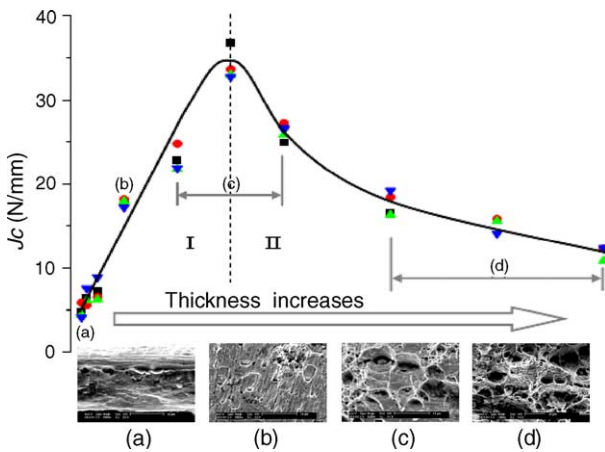


Fig. 10. Fracture toughness vs. thickness. (a) Brittle fracture occurs with shear mode fracture; (b) shear mode fracture occurs with ductile fracture with shallow dimples; (c) mixed ductile fracture with slip bands, tear ridges and lenticular dimples; (d) mixed ductile fracture with tear ridges and well-developed equiaxed dimples. This shows that fracture toughness is associated with the fracture mechanism.

4.2. Discussion of J_C versus thickness

The value of the fracture toughness J_C is the sum of the work required per unit area during crack-tip necking and the work required per unit area during material separation. The work required per unit area during crack-tip necking is related

to the degree of crack-tip necking. The work required per unit area during material separation is linked to the micro-fracture appearance. It is known that the work per unit area for crack-tip necking is greater at a larger degree of crack-tip necking and the work per unit area for material separation increases when the amount of slip bands and tear ridges increases. Moreover, the work per unit area for material separation in the case of ductile fracture is greater than that in the case of brittle fracture. Consequently, by comparing the degree of crack-tip necking, the micro-mechanisms of fracture and micro-fracture appearance, one might be able to qualitatively compare the value of fracture toughness J_C of the specimens with various thicknesses.

In stage I, results of macroscopic examination show that the degree of necking at the crack tip increases with increasing thickness in the macroscale. SEM micro-fractographs show that the fracture mechanism changes from a mixed brittle/shear-mode fracture (Fig. 8(a)) to a mixed shear-mode/ductile fracture (Fig. 8(b)), and then to a mixed ductile fracture with slip bands, tear ridges and lenticular dimples (Fig. 8(c and d)). In addition, in the case of ductile fracture (Fig. 8(c and d)), as the thickness increases, the amount of slip bands, tear ridges and the size of the dimples all increase. These above-mentioned fracture features indicate that both the work required per unit area for crack-tip necking and the work per unit area for material separation increase with increasing thickness. As a result, fracture toughness J_C , which is comprised of the above two contributions, increases with increasing thickness in stage I.

In stage II, however, the degree of crack-tip necking decreases with increasing thickness, and the fracture mechanism changes from mixed ductile fracture with slip bands, tear ridges and lenticular dimples (Fig. 9(a and b)) to mixed ductile fracture with tear ridges and well-developed equiaxed dimples only (Fig. 9(c and d)). Moreover, the amount of slip bands and tear ridges decreases with an increase in thickness. These fracture features show that an increase in thickness will lead to a decrease in both the work per unit area for crack tip necking and the work per unit area for material separation. Therefore, fracture toughness J_C decreases with an increase in thickness during stage II. It can also be explained by the influence of the stress triaxiality. Indeed, toughness is affected by the stress state. With increasing thickness, stress triaxiality will tend to increase at the crack tip, to accelerate the void growth rate, to decrease the fracture strain and crack-tip necking degree, and thus to lead to a decrease of fracture toughness J_C . This can justify results (e.g. Broek [25]) where the toughness is observed to decrease with increasing thickness even at small thicknesses.

4.3. Comparison between V-specimens and H-specimens

The results of macroscopic examination of the specimen surface showed evidence of roll marks along the rolling direction, and the grains are also elongated along the rolling direction. These two factors are thought to reduce the frac-

ture resistance and to be responsible for the fact that the J_C values of the V-specimens are always greater than those of the H-specimens provided their thicknesses are identical. Firstly, the presence of the roll marks indicates that the micro-defects occur along the rolling direction. In the case of the H-specimens, the direction of the roll marks is perpendicular to that of the tensile load and parallel to that of the main crack, so it is easy for micro-defects to induce coalescence of the inner or surface micro-cracks to form “macro-cracks” when subjected to tensile load. Furthermore, the grain flow direction is parallel to the main crack in the H-specimens (see Fig. 2). As a result, a crack in H-specimens is easier to initiate because the fracture plane follows the plane of lowest crack resistance, with less grain boundaries to cross [25].

5. Conclusions

A comprehensive experimental study of the effect of thickness on the fracture toughness of metallic foil has been carried out. Fracture toughness, characterized by J_C , of copper foils with thicknesses from 0.02 to 1 mm was evaluated using DSCM. Experimental results indicate that the value of J_C depends strongly on thickness.

Additionally, the metallographic examination results of the fracture surface and fracture profile of copper foil specimens demonstrate (i) a change in failure mode, from a more brittle mechanism to a more ductile mechanism involving void growth and (ii) a combined evolution of the degree of crack tip necking.

The significant effect of thickness is essentially attributed to the change in the work required per unit area during crack-tip necking and in the work required per unit area during material separation. The major factors affecting these two contributions and fracture features are considered to be related to the combined action of the microstructure, the presence of inner micro-defects and roll marks, and the level of stress triaxiality. And the effects of all the above-mentioned factors for fracture toughness might be different with different thickness.

Acknowledgements

This work is financially supported by the National Natural Science Foundation of China (No.10232030). The support is fully acknowledged.

Appendix A

In elasto-plastic fracture mechanics, the fracture criterion is based on the energy release rate, J integral proposed by Rice [26]. The J integral criterion has successfully been used to solve many practical fracture problems. In a non-linear

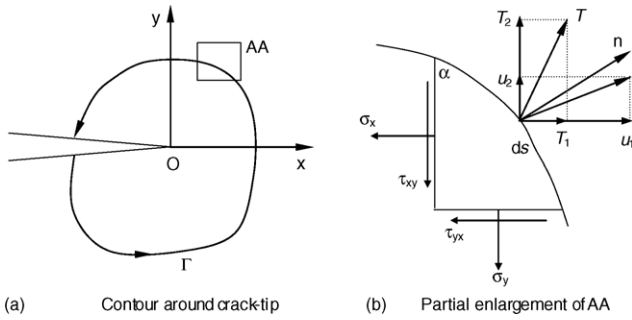


Fig. 11. Contour around crack-tip for calculating J integral. (a) Contour around crack-tip; (b) partial enlargement of AA.

elastic material the J integral is defined by

$$J = \int_{\Gamma} \left(w \, dy - T_i \frac{\partial u_i}{\partial x} \, ds \right), \quad (A.1)$$

where Γ is an anticlockwise contour that surrounds the crack-tip (see Fig. 11(a)), w the strain energy density, T_i component of the traction vector, u_i is a component of the displacement vector and ds is an element of Γ . The equilibrium equations of the triangular element of ds are

$$\left. \begin{aligned} n_1 &= \cos \alpha = \frac{dy}{ds} \\ n_2 &= \sin \alpha = -\frac{dx}{ds} \end{aligned} \right\}, \quad (A.2)$$

with

$$\left. \begin{aligned} T_1 &= \sigma_x n_1 + \tau_{xy} n_2 \\ T_2 &= \tau_{xy} n_1 + \sigma_y n_2 \end{aligned} \right\}, \quad (A.3)$$

where n_1 and n_2 are the direction cosines of the outer normal vector of the arc element ds , as shown in Fig. 11(b).

Moreover, for a small scale yielding case and under the framework of linear elastic mechanics, we have

$$\left. \begin{aligned} w &= \frac{1}{2}(\sigma_x \varepsilon_x + \sigma_y \varepsilon_y + \tau_{xy} \gamma_{xy}) \\ \sigma_x &= \frac{E}{1 - \mu^2}(\varepsilon_x + \mu \varepsilon_y) \\ \sigma_y &= \frac{E}{1 - \mu^2}(\varepsilon_y + \mu \varepsilon_x) \\ \tau_{xy} &= G \gamma_{xy} \end{aligned} \right\}. \quad (A.4)$$

Substituting (A.2)–(A.4) into (A.1) yields Eq. (2) in Section 2. With Eq. (2), the J integral can be calculated using the digital correlation data.

References

- [1] M.A. Sutton, J.L. Turner, Y.J. Chao, H.A. Bruck, T.L. Chae, *Int. J. Fract.* 53 (1992) 201–228.
- [2] M. Judelewicz, H.U. Kunzi, N. Merk, B. Ilschner, *Mater. Sci. Eng. A* 186 (1994) 135–142.
- [3] E. Arzt, *Acta Mater.* 46 (1998) 5611–5626.
- [4] Z.Y. Fan, *Mater. Sci. Eng. A* 191 (1995) 73–83.
- [5] Q. Zhou, G. Itoh, T. Yamashita, *Mater. Trans. JIM* 40 (1999) 443–446.
- [6] S. Hong, R. Weil, *Thin Solid Films* 283 (1996) 175–181.
- [7] H.D. Merchant, M.G. Minor, Y.L. Liu, *J. Electron. Mater.* 28 (1999) 998–1007.
- [8] D.T. Read, *Int. J. Fatigue* 20 (1998) 203–209.
- [9] A. Hadrboletz, B. Weiss, G. Khatibi, *Int. J. Fract.* 107 (2001) 307–327.
- [10] M. Klein, G. Khatibi, B. Weiss, *Mater. Sci. Eng. A* 319–321 (2001) 924–928.
- [11] Y. Choi, S. Suresh, *Acta Mater.* 50 (2002) 1881–1893.
- [12] T. Pardoen, Y. Marchal, F. Delannay, *J. Mech. Phys. Solids* 47 (1999) 2093–2123.
- [13] T. Pardoen, Y. Marchal, F. Delannay, *Eng. Fract. Mech.* 69 (2002) 617–631.
- [14] T. Pardoen, J.W. Hutchinson, *Acta Mater.* 51 (2003) 133–148.
- [15] I. Yamaguchi, *Opt. Acta* 28 (1981) 1359–1376.
- [16] W.H. Peters, W.F. Ranson, *Opt. Eng.* 21 (1982) 427–431.
- [17] H. Lu, G. Vendroux, W.G. Knauss, *Exp. Mech.* 37 (1997) 433–439.
- [18] H. Lu, P.D. Cary, *Exp. Mech.* 40 (2000) 393–400.
- [19] H.W. Wang, Y.L. Kang, *Opt. Eng.* 41 (2002) 2793–2798.
- [20] H.W. Wang, Y.L. Kang, Z.F. Zhang, Q.H. Qin, *Int. J. Fract.* 123 (2003) 177–185.
- [21] F.Q. Yang, *Mater. Sci. Eng. A* 358 (2003) 226–232.
- [22] A. Kotousov, P.J. Tan, *Int. J. Fract.* 197 (2004) 97–103.
- [23] S.M. El-Soudani, *J. Miner. Met. Mater. Soc.* 42 (1990) 20–27.
- [24] M.F. Kanninen, C.H. Popelar, *Advanced Fracture Mechanics*, Oxford University Press, New York, 1985.
- [25] D. Broek, *Elementary Fracture Mechanics*, third revised ed., Martinus Nijhoff Publishers, Boston, 1986.
- [26] J.R. Rice, *J Appl. Mech.* 35 (1968) 379–386.